nature communications

Article

https://doi.org/10.1038/s41467-024-52770-z

Halogenated-edge polymeric semiconductor for efficient spin transport

Received: 10 March 2024

Accepted: 19 September 2024

Published online: 27 September 2024

Check for updates

Xueli Yang[1,2,3,7], Ankang Guo[1,2,3,7], Jie Yang[1,7], Jinyang Chen[1], Ke Meng[2,3], Shunhua Hu[2,3], Ran Duan[4], Mingliang Zhu[1,3], Wenkang Shi[1,3], Yang Qin[2,3], Rui Zhang[5], Haijun Yang[6], Jikun Li[3,4], Lidan Guo[2,3] ✉, Xiangnan Sun[2,3] ✉, Yunqi Liu[1,3] ✉ & Yunlong Guo[1,3] ✉

Organic semiconductors (OSCs) are featured by weak spin-orbit coupling due to their light chemical element composition, which enables them to maintain spin orientation for a long spin lifetime and show significant potential in room-temperature spin transport. Carrier mobility and spin lifetime are the two main factors of the spin transport performance of OSCs, however, their ambiguous mechanisms with molecular structure make the development of spintronic materials really stagnant. Herein, the effects of halogen substitution in bay-annulated indigo-based polymers on carrier mobility and spin relaxation have been systematically investigated. The enhanced carrier mobility with an undiminished spin lifetime contributes to a 3.7-fold increase in spin diffusion length and a record-high magnetoresistance of 8.7% at room temperature. By analyzing the spin-orbit coupling and hyperfine interaction, it was found that the distance of the substitution site from the conjugated center and the nitrogen atoms in the molecules play crucial roles in spin relaxation. Based on the above results, we proposed a molecular design strategy of halogen substitution far from conjugate center to enhance spin transport efficiency, presenting a promising avenue for advancing the field of organic spintronics.

Spintronics, utilizing spin degree of freedom for information storage, transport and processing, have greatly triggered the development of information technology[1–5]. Efficient spin transport in spintronic channel materials is the prerequisite for fundamental scientific research and achieving various spin-related functionalities, which require the charge carriers to maintain their spin orientation for as long or as far as possible[6–11]. At this request, the channel materials with long spin lifetime at room temperature would be attractive in practical applications, since the spin scattering will aggravate along with increasing temperature[12–14]. Organic semiconductors (OSCs) composed of atoms with low atomic numbers (such as C, H, etc.) possess weak spin-orbit coupling (SOC) and thus relatively long spin lifetime at room temperature[15–18], due to the SOC strength is proportional to the fourth power of atomic numbers[19]. In addition, the unique chemical tailorability and optoelectronic properties of OSCs coupled with their effective spin transport property further triggered the utilization of OSCs in multipurpose spintronic devices[20–26]. These

[1]Beijing National Laboratory for Molecular Sciences, Key Laboratory of Organic Solids, Institute of Chemistry Chinese Academy of Sciences, Beijing 100190, P. R. China. [2]Key Laboratory of Nanosystem and Hierarchical Fabrication, CAS Center for Excellence in Nanoscience, National Center for Nanoscience and Technology, Beijing 100190, P. R. China. [3]University of Chinese Academy of Sciences, 100049 Beijing, P. R. China. [4]Beijing National Laboratory for Molecular Sciences, Key Laboratory of Photochemistry, Institute of Chemistry, Chinese Academy of Science, Beijing 100190, P. R. China. [5]Beijing Key Laboratory of Microstructure and Property of Solids, Faculty of Materials and Manufacturing, Beijing University of Technology, Beijing 100124, P. R. China. [6]Department of Chemistry, Tsinghua University, 100084 Beijing, P. R. China. [7]These authors contributed equally: Xueli Yang, Ankang Guo, and Jie Yang.
✉e-mail: guold@nanoctr.cn; sunxn@nanoctr.cn; liuyq@iccas.ac.cn; guoyunlong@iccas.ac.cn

factors collectively drive organic spintronics as an independent and widely researched field with substantial potential.

In organic spintronics, spin transport is considered as the most central and concerned research content. Improving the spin transport efficiency of OSCs is a long-term pursuit, and the investigation of the molecular structure of OSCs should be the most fundamental way to realize this aim. According to the spin diffusion length (λ_s) relationship:

$$\lambda_s = \sqrt{\mu k_B T \tau / e} \quad (1)$$

where μ, K_B, T, τ and e are the carrier mobility, Boltzmann constant, temperature, spin lifetime and the charge constant, respectively[14,27,28]. It is clearly observed that the mobility and spin lifetime of OSCs should be equally important to the spin diffusion length. However, many investigations focus only on exploring the relationship between element composition and molecular structure of OSCs and their spin lifetime, ignoring the effect on mobility or simply assuming no effect[15,16,29–31]. In contrast, in the study of improving the mobilities of OSCs in organic electronics, the influence of molecular structure change on spin lifetime has been ignored in a long period. Generally, the design of traditional high-mobility OSCs mainly introduces some electron-withdrawing or electron-donating groups into the molecular skeleton to modulate the electrical properties of the material[32,33]. However, most of the introduced groups contain magnetic nuclei (such as H, N, and F) or heavy atoms (Cl, S, and Se)[34–37], which is thought to alter the spin relaxation environment and thus spin lifetime within the molecule[12,15,18,38]. Unfortunately, the spin-flipping mechanism of many π-conjugated materials is not yet better understood, and their microscopic interactions remain elusive, especially for nitrogen-containing π-conjugated molecular systems with high carrier mobility. The absence of comprehensive studies on the effects of molecular structure on spin transport and relaxation mechanisms results in the lack of theoretical guidance for molecular structure design, which has greatly hindered the development of organic spintronic materials.

Considering the introduction of electron-withdrawing groups into the molecular skeleton is the most typical approach to modulating electron mobility, herein, bay-annulated indigo (BAI)-based polymers with many active sites were taken as the research object, and a series of polymers by halogen substitution were designed and synthesized. As expected, the mobilities of BAI-based polymers increased by more than one order of magnitude with the increase of substituent groups. However, unexpectedly, the spin lifetime of these molecules, precisely measured by pulsed electron paramagnetic technology, has been found not to decreased as the number of substituent groups increased. By respective and detailed analysis of the spin relaxation mechanisms from the micro-interaction of the substituents, together with DFT calculations, it was found that the influence of substituents on spin relaxation is closely related to the distance of substituents from the conjugated center of the molecules. When halogen groups are substituted in the edge region far from the conjugated center of molecules, the influence of introduced halogen groups on spin density distribution, SOC and hyperfine interaction (HFI) strength was very weak. Therefore, the mobility can be increased without reducing the spin lifetime. In this case, the spin diffusion length of the molecules whose edge is replaced by halogen has been improved by more than three times compared to the original molecules. Such results can provide a molecular design strategy for overall improving spin transport distance, and will open an avenue for organic spintronic study from a molecular design way.

Results

Synthesis and characterizations of halogen-substituted BAI-based polymers

At present, the introduction of electron-withdrawing groups to regulate the energy level of OSCs is an effective strategy for modulating carrier mobility. Among them, halogen substitution is a typical method[39–42], which can not only regulate the energy level of the materials but also optimize their crystallinity and solubility. BAI unit[43–46] is an excellent building block for studying halogen substitution since there are eight hydrogen atoms with similar chemical environments on both sides of the BAI unit, which provides the possibility for molecular synthesis and quantitative halogen substitution. In addition, BAI derivatives commonly possess excellent solution processing performance and electrical properties, which is beneficial for constructing spintronic devices. Herein, we use a novel two-step synthesis method to effectively introduce various halogen atoms into BAI units at different substitution positions. As shown in Fig. 1a, BAI units containing electron-withdrawing groups have been synthesized. Finally, **7a** (PBAI-V), **7b** (P2ClBAI-V) and **7c** (PFClBAI-V) have been prepared via traditional stille polymerization.

The Ultraviolet-visible absorption spectra of BAI-based polymers were measured in thin films, as shown in Fig. 1b. The absorption maxima (λ_{max}) of BAI-based polymers showed an obvious redshift from 778 nm to 917 nm with the increase of the number of halogen atoms. Furthermore, we also tested the material films' LUMO/HOMO energy levels (Supplementary Fig. 4) by low energy inverse photoelectron spectroscopy (LEIPS) and ultraviolet photoelectron spectroscopy (UPS). Supplementary Fig. 5 gives the energy level diagram of the organic layer. With the introduction of the electron-withdrawing group, the energy level of BAI-based polymers has undergone a significant downward shift. In fact, halogenated BAI units could exhibit stronger electron-withdrawing behaviors and thus corresponding halogenated polymer would enhance intramolecular push-pull interactions between BAI units and neighboring thiophenes. In this case, we further study the influence of halogen substitution on the carrier mobility of BAI-based polymers thin films by space charge limiting current method. Firstly, to eliminate the effect of the film's crystallinity on carrier mobility as much as possible, trichloromethane with a lower boiling point was selected as the solvent for the three materials without annealing. Through GI-XRD data (Supplementary Fig. 6), we determined that the material's film morphology is amorphous. According to the curves of current density versus voltage as shown in Fig. 1c, the electron carrier mobility in the vertical direction of PBAI-V, P2ClBAI-V, and PFClBAI-V is 0.98×10^{-4} $cm^2V^{-1}s^{-1}$, 3.2×10^{-4} $cm^2V^{-1}s^{-1}$ and 12.7×10^{-4} $cm^2V^{-1}s^{-1}$, respectively (Fig. 1d). Compared with the mobility of PBAI-V, the carrier mobility of P2ClBAI-V is increased by three times, and the mobility of PFClBAI is increased by one order of magnitude.

Spin-relaxation time of BAI-based polymers

To investigate the effect of halogenated-edge substitution on the spin relaxation of BAI-based polymers, pulsed electron paramagnetic resonance (EPR) as the most authoritative means is used to directly capture the spin precession and obtain accurate time parameters[47–49]. The spin-relaxation time includes the spin-lattice relaxation time T_1 and the spin-spin relaxation time T_2. T_1 is the time constant characterizing the recovery process of the longitudinal component, that is, the spin lifetime of the spin-polarized carrier in the material. It is an irreversible energy loss process that completed by the energy transfer between the spin center and the surrounding environment. The spin relaxation time T_1 is tested using an inversion recovery sequence[50], and the motion can visualize the quantum evolution of the spin on a Bloch sphere. The zenith position corresponds to the spin-up and spin-down states, respectively, and all quantum evolution processes are mapped onto the sphere (Fig. 2a). When we apply a π pulse, the spin in the material is reversed from top to bottom position (diagram I to II in Fig. 2a). And then the spin gradually evolves to the initial state as time t increases (diagram III in Fig. 2a). As shown in Fig. 2b, the intensity of the spin-echo increases with increasing t. By fitting the exponential

function[48]:

$$I(t) = A\left(1 - 2e^{-\frac{t}{T_1}}\right) \quad (2)$$

where I is the strength of the spin echo, A is the initial strength of the spin echo, and t is the recovery time, respectively. We obtain the T_1 of PBAI-V, P2ClBAI-V, and PFClBAI-V as 23.9 μs, 21.4 μs and 19.7 μs (Fig. 2c), respectively, which indicates a slight decrease of T_1 along with halogen substitution increased.

T_2 is the time constant characterizing the recovery process of the lateral component. This process is completed by energy relay transfer from the spin center, which does not involve energy loss and is a reversible process. In this study, we test T_2 using the Hahn echo sequence (see orange diagrams in Fig. 2a, IV to VIII corresponds to the evolution of the electron's spin), in which the intensity of the spin echo decreases with increasing τ (Fig. 2d). By fitting an exponential decay formula:

$$I(t) = Ae^{-\frac{t}{T_2}} \quad (3)$$

where I is the strength of the spin echo, A is the initial strength of the spin echo, and t is the free precession time ($t = 2\tau$). We extracted T_2 of PBAI-V, P2ClBAI-V and PFClBAI-V as 579 ns, 566 ns and 489 ns (Fig. 2e), respectively. The experimental results indicate that when hydrogen atoms at X_1 sites in the BAI unit are replaced by two Cl atoms (Fig. 1a), the spin relaxation time T_2 decreases by 13 ns, suggesting that Cl atoms have little effect on spin relaxation. However, after substituting two F atoms and two Cl atoms, T_2 of PFClBAI-V was significantly shortened by 90 ns compared with PBAI-V. The experimental findings clearly demonstrate that such halogen substitution has a slightly negative effect on the spin lifetime of the material. It is worth noting that the spin relaxation times of BAI-based polymers are all measured in solid films and at room temperature, which can better reflect the spin relaxation changes of materials in spin-related devices.

Spin diffusion length of BAI-based polymers

Spin diffusion length, as one of the important properties of OSCs, is closely related to both spin lifetime and mobility. Results shown in Fig. 1 and Fig. 2 reveal that the mobilities improved by an order, and the spin lifetimes did not go down obviously along with the increase of halogen substitution. Accordingly, calculated by the formula (1), λ_s of PBAI-V, P2ClBAI-V, and PFClBAI-V are 77 nm, 133 nm and 254 nm, respectively, which has been greatly improved along with the increase of the number of halogen substitution. About 170% and 330% enhancements of λ_s have been achieved in P2ClBAI-V and PFClBAI-V, respectively, compared to the non-substituted PBAI-V. Such results preliminarily prove that our designed halogen-substituted BAI-based polymers can significantly improve the carrier mobility without decreasing the spin relaxation time, and finally enhance the spin diffusion length.

To further demonstrate the enhancement of spin transport efficiency of these BAI-based polymers after halogen substitution, a spin valve, the most typical spintronic device for studying spin transport efficiency of channel materials, has been utilized. The spin valve used in the study is a vertical sandwich structure, in which the BAI-based polymeric film is sandwiched between the two ferromagnetic (FM) electrodes (Co and NiFe)[51]. In such device, spin-polarized carriers are injected from one of the FM electrodes driven by a bias voltage, followed by transport and spin relaxation in BAI-based polymer layer, and finally detected by the other FM electrode. The spin transport efficiency of BAI-based polymers can be characterized as magnetoresistance, $MR = (R_{AP} - R_P)/R_{AP} \times 100\%$, where R_{AP} and R_P are the device resistances when the two FM electrodes are aligned as antiparallel and parallel, respectively[3]. In our study, the spin valve structured by Co (20 nm)/AlO_x (1.7 nm)/Polymer/NiFe (12 nm) from bottom to top is

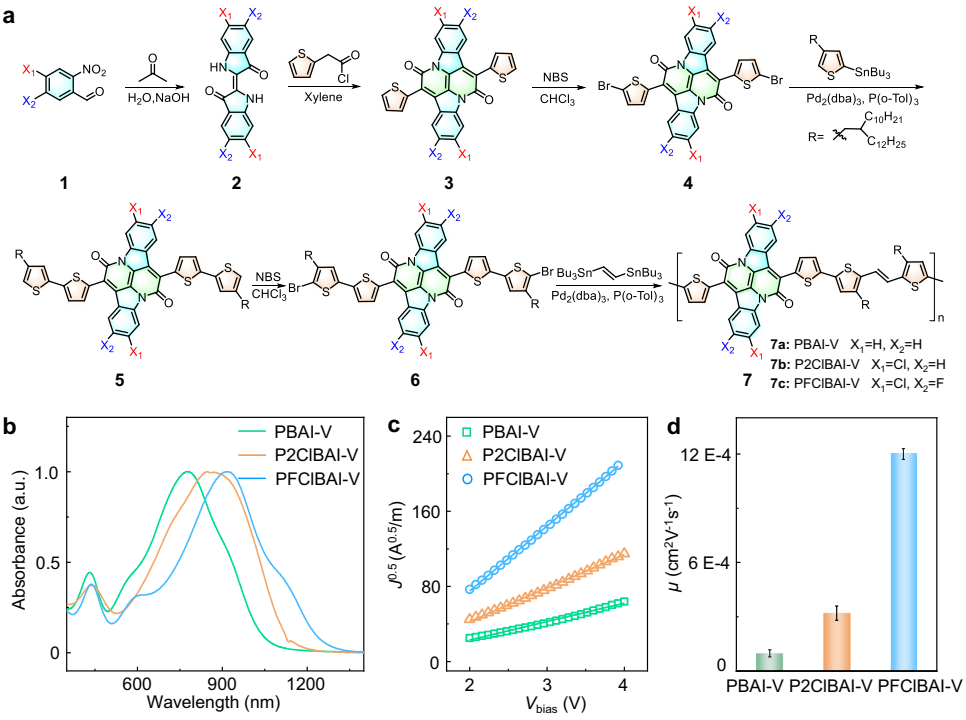

Fig. 1 | Molecular synthesis and characterization of BAI-base polymers. a The synthesis route of BAI-based polymers consists of six steps. Compounds **1**–**5** serve as the raw material molecules, and the synthesis methods for compounds **6** and **7** are provided in the Supplementary Information. **b** Ultraviolet-visible absorption spectra of BAI-based polymers in thin film. **c** Experimental (hollow icons) and fitted (solid lines) current density–voltage characteristics of ITO/Polymer/LiF/Al devices. **d** Carrier mobility of BAI-based polymers measured by space charge limited current (SCLC) method. Error bars indicate that data are collected from five devices on the same chip.

https://doi.org/10.1038/s41467-024-52770-z

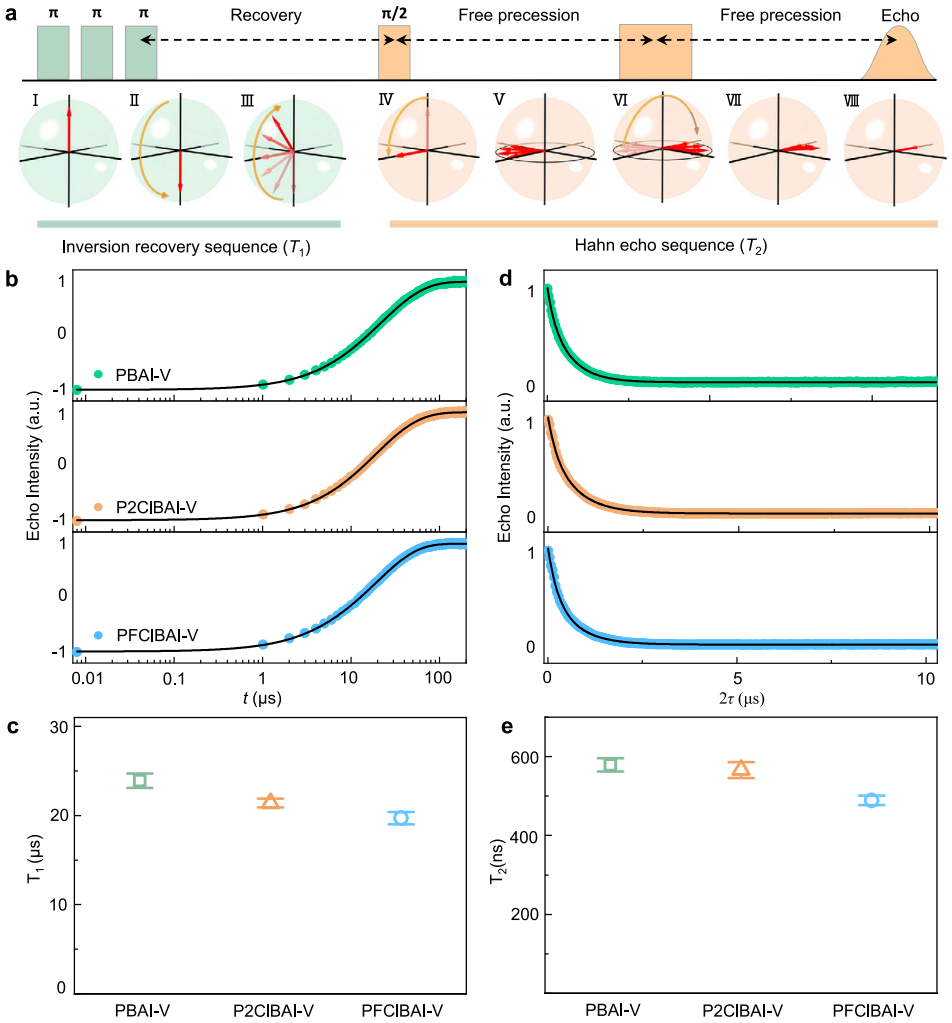

Fig. 2 | Spin relaxation time of BAI-based polymers at room temperature. **a** Pulse sequence of ESR used to extract the spin-lattice and coherence times (top panel), and the spin evolution in Bloch spheres corresponding to above pulse sequence (bottom panel). I to VIII represent the evolution state after the action of different pulses. The green and orange sections represent the testing and evolution of spin relaxation times T_1 and T_2, respectively. **b** The inversion recovery curves measured in PBAI-V, P2ClBAI-V and PFClBAI-V thin films. Black lines are the fitted result according to the circular data points. The green, tan, and blue circular dots represent the experimental data collected by PBAI-V, P2ClBAI-V, and PFClBAI-V, respectively. **c** The spin relaxation time T_1 extracted from (**b**). **d** Hahn-echo signal versus the free precession time τ for PBAI-V, P2ClBAI-V and PFClBAI-V. Black lines are the fitted result according to the circular data points. The green, tan, and blue circular dots represent the experimental data collected by PBAI-V, P2ClBAI-V, and PFClBAI-V, respectively. **e** The spin relaxation time T_2 extracted from (**d**). The error bars in (**c**) and (**e**) indicate that the data are collected from five measurements of the same sample.

shown in Fig. 3a. Among them, the role of AlO_x is to isolate the contact between Co and the organic layer and prevent interfacial hybridization between the active Co and the organic molecules. In addition, to eliminate the effect of the thin film microstructure on spin properties as much as possible, we used the same film preparation process as the carrier mobility test. As shown in Supplementary Fig. 7, the 50 nm BAI-based polymers coated on the AlO_x layer have very smooth morphology and root mean square roughness (R_q) < 1 nm. Meanwhile, to suppress the penetration damage of the polymer layer originating from the top electrode evaporation and thus improve the credibility of device performance, low-temperature deposition technology has been used for preparing the top NiFe electrodes[52]. The interface between the polymer intermediate layer and the NiFe electrodes can be found very smooth and clear through the transmission electron microscope and energy dispersive X-ray spectroscopy (EDS), as shown in Fig. 3b, c, indicating the interfacial penetration is negligible and the consistent evaluation of the BAI polymer performance can be ensured.

As shown in Fig. 3d, the *MR* signals of spin valves based on PBAI-V, P2ClBAI-V, and PFClBAI-V are 2.9%, 4.6% and 8.7% at room temperature, respectively. Notably, the spin transport efficiency of BAI-based polymers is significantly improved with the increase of substitution of halogen groups into BAI-based polymers, and the *MR* of 8.7% at room temperature is a highest record reported so far. Furthermore, the *MR* of spin valves based on different thicknesses of BAI-based polymers has been measured, and accordingly, the spin diffusion length λ_s have been extracted by fitting the thickness-dependent *MR* response via the modified Julliére model[3]:

$$MR = \frac{R_{AP} - R_P}{R_{AP}} = \frac{2P_1P_2e^{-(d-d_0)\lambda_s}}{1+P_1P_2e^{-(d-d_0)\lambda_s}} \quad (4)$$

where d is the thickness of the organic layer between the FM electrodes, and d_0 is the thickness of the ill-defined layer. P_1 and P_2 are the injected and detected spin polarizability at the side of the spacer, respectively. Figure 3e shows the fitting results of the *MR* response with different thicknesses of BAI-based polymers at room temperature. The λ_s of PBAI-V, P2ClBAI-V, and PFClBAI-V are 63 nm, 141 nm, and 247 nm, respectively. Such results are also very close to

https://doi.org/10.1038/s41467-024-52770-z

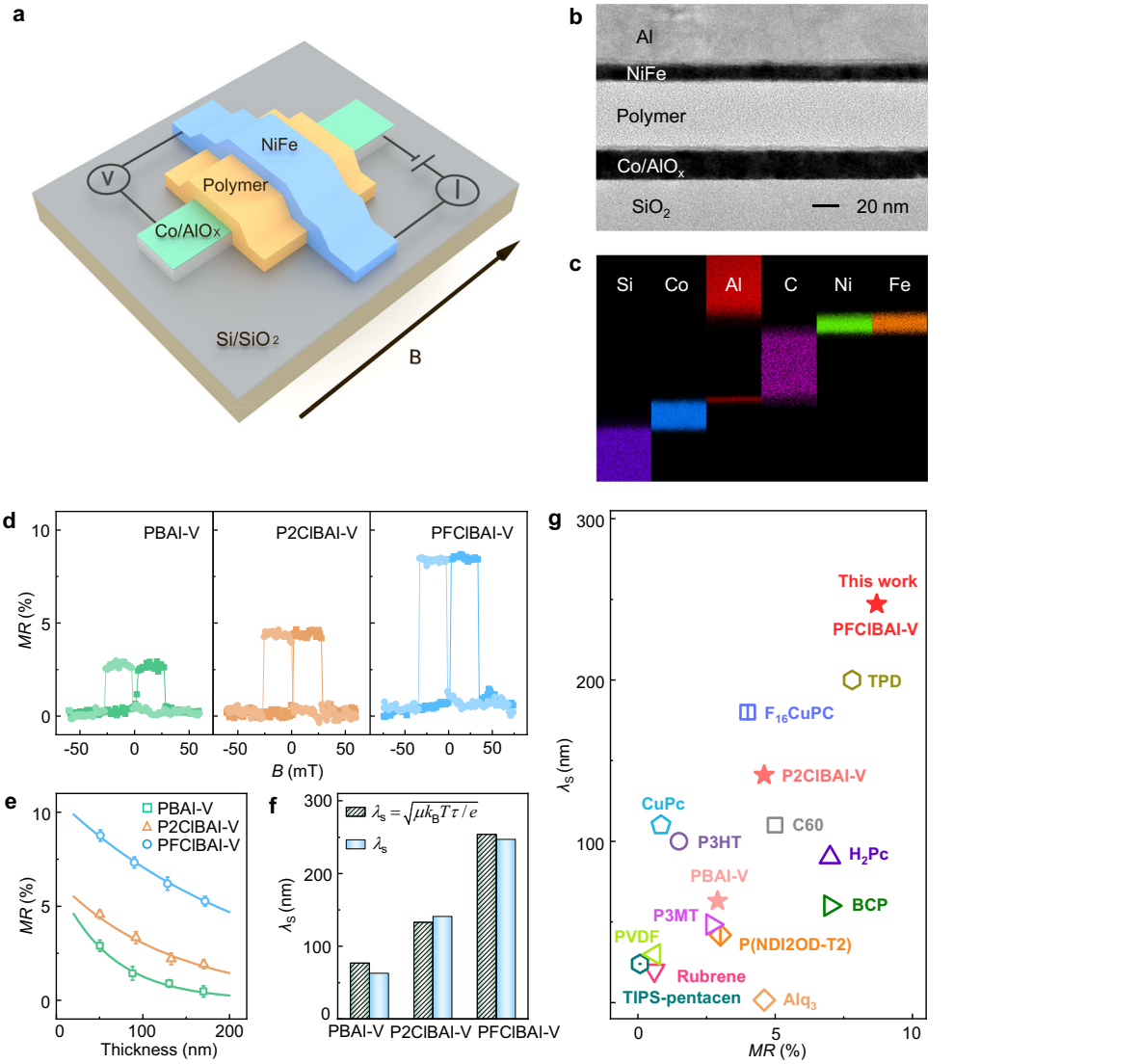

Fig. 3 | Spin diffusion length of BAI-based polymers at room temperature. **a** Schematic diagram of BAI-based polymers spin valve. **b** A cross-sectional transmission electron microscope image and (**c**) The corresponding elementary mapping by EDS of the spin valve structure. **d** Magnetoresistance curves of spin valves with 50 nm-thick BAI-based polymers at room temperature. The bias voltage was fixed at 10 mV to measure the magnetoresistance effect. Note that all the *MR* tests in this article are measured by a sweeping magnetic field from negative to positive (corresponding to the right peak of curves) to negative (corresponding to the left peak of curves). **e** Thickness-dependent *MR* of spin valves based on PBAI-V, P2ClBAI-V, and PFClBAI-V, respectively. The solid lines are the fitted curves according to formula (4). Error bars indicate the data are collected from five devices on the same chip at each thickness. **f** Comparison of the spin diffusion length of PBAI-V, P2ClBAI-V, and PFClBAI-V, green pattern bar chart represents λ_s calculated by formula (1) and blue bar chart represents λ_s fitted by formula (4). **g** Comparison of *MR* and λ_s of BAI-based polymers with other organic materials at room temperature reported in the literature. The same color used for both the icon and font represents the corresponding molecular semiconductor material. Details of data points are presented in Supplementary Table 2.

the value of the spin diffusion lengths calculated by formula (1). A summary of spin diffusion lengths achieved by these two methods can be seen in Fig. 3f and Supplementary Table 1. The detection of a room-temperature *MR* signal in the spin valve is mainly related to the thickness of the organic interlayer and electrode selection. We summarize the organic semiconductors that have been reported and achieved room-temperature spin transport so far (see Supplementary Table 2 for details)[52–64]. It is clearly observed that the room-temperature *MR* signal of the spin valve using an LSMO electrode is relatively small, and the maximum is only 3%. The reason is that the Curie temperature of the LSMO electrode is relatively low ($T_C \approx 360$ K), and it is difficult to achieve spin injection at room temperature. However, ferromagnetic electrodes with high Curie temperatures ($T_C > 800$ K), such as NiFe, Co, and Fe, can achieve spin injection and transport at room temperature even if the spin polarization ratio of the electrode is only 30 to 40%. In addition, the thickness of the organic interlayer is also a direct factor affecting the room temperature *MR* Signal. However, the thickness of spin devices used for each material is different, making it difficult to compare the spin properties of materials. Spin diffusion length, as an essential parameter to describe the spin transport properties of materials, provides the possibility for the performance comparison between different materials. As shown in Fig. 3g, our BAI-based polymers show the long spin diffusion length and *MR* in non-doped and non-single-crystal organic semiconductors at room temperature. All these results make sure that our designed BAI-based polymers enable to obviously improve the spin diffusion length.

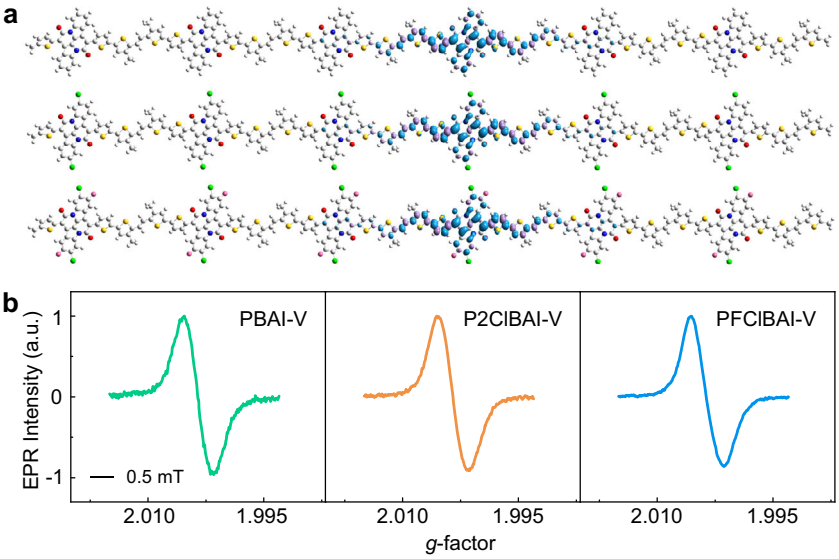

Fig. 4 | Spin density distribution and *g*-factor of BAI-based polymers at room temperature. a Spin density distribution of PBAI-V (top), P2ClBAI-V (middle) and PFClBAI-V (bottom) (where $n = 6$). The DFT calculations were performed at the CAM-B3LYP/6-31 G* level. The colors of the atoms: gray for C, red for O, blue for N, yellow for S, white for H, pink for F, and green for Cl. **b** Derivative electron paramagnetic resonance (EPR) spectra of PBAI-V (green line), P2ClBAI-V (tan line), and PFClBAI-V (blue line) at room temperature.

Discussion

Spin density distribution of BAI-based polymers

The above results reveal that the introduction of halogen atoms with high spin relaxation causation in BAI-based polymers does not result in an apparent decrease in spin lifetime, which is somewhat surprising. An investigation into the intrinsic mechanism of such results will surely be meaningful for further revealing the spin relaxation mechanisms in OSCs and opening avenues for the design of efficient spin transport materials. In OSCs, SOC and HFI are the main spin relaxation mechanisms to affect the spin lifetimes. Therefore, an analysis of the changes in SOC and HFI (or the lack thereof) should reveal the reasons why that the spin lifetimes of P2ClBAI-V and PFClBAI-V are in line with PBAI-V despite the halogen substitutions. In addition, spin density distribution describes the probability density of finding electrons with a particular spin orientation in a specific region of space, which is mainly influenced by SOC and HFI strength in molecules[18,65]. The changes in chemical element compositions and spatial geometry in OSCs are likely to result in changes in the spin relaxation environment with a high probability.

To investigate the spin density distribution of BAI-based polymers, we first explored the origin of their radicals using EPR technology. As shown in Supplementary Fig. 8, we added paraxylene to a solid sample, and as the material dissolved, the EPR signal completely disappeared. It shows that the single chain of BAI-based polymers itself may not exist free radicals. Subsequently, the BAI-based polymer was tested using EPR under nitrogen protection. As shown in Supplementary Fig. 9, the EPR signal showed a rapid decline. The results indicated that air was an essential source of radicals for BAI-based polymers. This phenomenon is consistent with the recently reported results of trace oxygen in organic semiconductors[66]. Furthermore, we scanned the EPR signal from 160 mT to 175 mT at room temperature and 100 K (Supplementary Fig. 10 and 11) and did not observe a half-field signal[67], thereby excluding the possibility of BAI-based polymers exhibiting an open-shell biradical character. Given that this study primarily focuses on the spin properties of BAI-based polymers for electron transport, we employed density functional theory (DFT)[68,69] to calculate the spin density in the anionic radicals of BAI-based polymers. The calculation results are shown in Fig. 4a. It is found that the spin density is mainly distributed on the conjugated skeleton (that is, the BAI unit) of the molecules. However, different from the substitution of specific functional groups into the skeleton sites of molecules in the traditional molecular design strategies (whose SOC and HFI will be greatly influenced by substituted groups), the change of spin density in BAI-based molecules along with the degree of halogen substitution can almost be negligible. We note that the halogen substitution sites are at the edge of the conjugated skeletons, far from the center of the conjugated BAI unit, which may lead to a very low coupling probability between the substituted halogens and spins at the conjugated skeleton center. Therefore, we assume that the variation of the edge elements of the conjugate skeleton has little effect on the spin density distribution in the molecule, and thus the introduced F and Cl atoms play an almost negligible role in the change of spin density distribution.

SOC of BAI-based polymers

To further confirm the origin of the almost unchanged spin lifetimes of BAI-based polymers with increasing degree of halogen substitution, the SOC and HFI strength have been respectively characterized by continuous-wave electron paramagnetic technique. It is well known that the *g*-factor can reflect the change in the SOC of the material, and the formula is as follows:

$$\Delta g = \Delta g^{\mathrm{RMC}} + \Delta g^{\mathrm{GC}} + \Delta g^{\mathrm{OZ/SOC}} \tag{5}$$

where Δg^{RMC} is the relativistic mass correction, Δg^{GC} represents the diamagnetic gauge correction, $\Delta g^{\mathrm{OZ/SOC}}$ is the cross-term of the orbital Zeeman and SOC operators, corresponding to the mixed derivative of the total molecular energy with respect to the electron magnetic moment and the external magnetic field[15]. Usually, the first two terms are minimal and cancel each other out, so $\Delta g^{\mathrm{OZ/SOC}}$ is the main factor determining the change in the *g*-factors. In the EPR spectra of BAI-base polymers (Fig. 4b), only a single peak with a peak width of 0.6 mT has been observed at room temperature. Through the EPR data, we extracted the *g*-factors of PBAI-V, P2ClBAI-V, and PFClBAI-V as 2.0036, 2.0035, and 2.0037, respectively. Therefore, the *g*-factor changes by no more than 50 p.p.m. with the increase of halogen atoms, proving that the effect of halogenated edge substitution on BAI-based polymer SOC is almost negligible.

https://doi.org/10.1038/s41467-024-52770-z

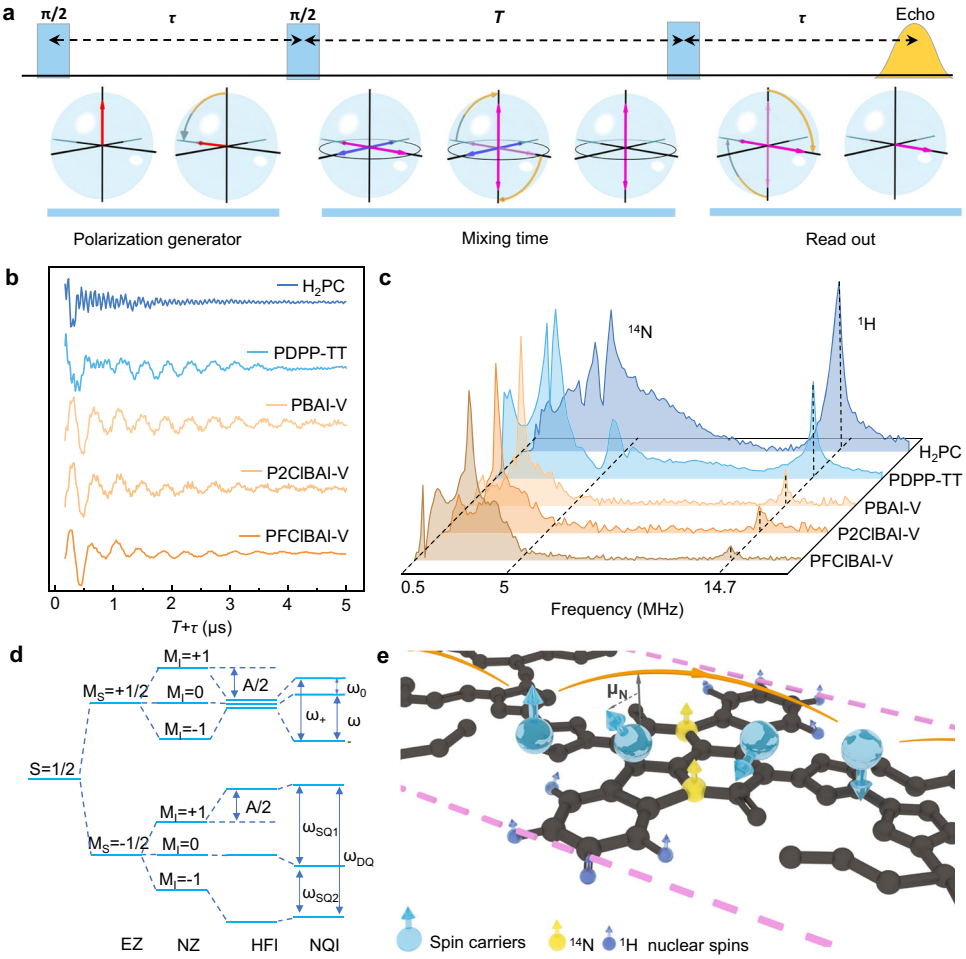

Fig. 5 | HFI of BAI-based polymers at room temperature. a Schematic diagram of stimulated echo sequence of 3P-ESEEM[70]. Electron coherence is generated by π/2-*T*-π/2 pulse sequence (Polarization generator). After time *T*, electron and nuclear spins are mixed, and the spin echo signal is modulated periodically (Mixing time). Finally, the π/2-*T*-π/2 pulse sequence is applied to read out the signal (Read out). **b** Echo signals of H_2PC, PDPP-TT, PBAI-V, P2ClBAI-V and PFClBAI-V with mixing time *T*, respectively. The blue curve represents the echo signal of H_2PC and PDPP-TT, and the yellow curve represents the echo signal of BAI-based polymers. **c** Frequency domain spectrum of echo signal after Fourier transform. **d** The energy level diagram with an $S = 1/2$, $I = 1$ spin system under the condition of exact cancellation ($|A/2| = |\nu_I|$). (EZ electron Zeeman interaction, HFI hyperfine interaction, NZ nuclear Zeeman interaction, NQI nuclear quadrupole interaction, SQ single quantum, and DQ double quantum). **e** Schematic representation of the spin-relaxation interaction, in which the azure sphere represents the spin-polarized charge carriers, the yellow and blue sphere represents the nuclear spins of the ^{14}N and ^{1}H atoms, and the μ_N is the nuclear magnetic moment from the nuclear spins of the ^{14}N and ^{1}H atoms.

HFI of BAI-based polymers

To understand the effect of HFI on spin relaxation in thin-film materials at room temperature, we used the electron spin-echo envelope modulation (ESEEM) technique to explore the deeper interaction mechanism. The basic principle of ESEEM technique[70–72] is to detect the dynamic changes of the echo intensity of the spin signal as the pulse time interval (*T*) gradually increases. Suppose all the nuclear spins in the material are zero ($I = 0$). In that case, the electron spin echo will decay exponentially with *T*. If one or more magnetic nuclei exist in the material ($I \geq 0$), the echo intensity is not only attenuated by the envelope exponentially with *T*, but also affected by the modulation of the nuclear spin transition frequency. The advantage of this method is that if there is HFI between magnetic nuclei and spin-polarized electrons, the nuclear frequency will modulate the spin-echo signal, so this technology can effectively detect the spin relaxation information inside molecules.

The standard three-pulse ESEEM (3P-ESEEM) has been used to detect the HFI effects in BAI-based polymers with the same solid weight, where the applied pulse sequence is π/2-τ-π/2-*T*-π/2-τ−echo. As shown in Fig. 5a, we present the evolution of spins on Bloch spheres. After the first π/2 pulse is given, the stimulated echo in vibration attenuation along with the mixing time (*T*) between the second and third pulse[73]. Figure 5b shows the spin-echo data with the exponential decay deducted. The modulation of the spin echo shows two different modulation characteristics, one of which is featured by large amplitude and small frequency, and the other one presents small amplitude and high modulation frequency. It indicates that the spin-polarized electrons in the material system are subjected to the hyperfine coupling of two different modulation frequencies. Generally, the Larmor precession information of the magnetic core in the original data is encoded as a modulated signal, and the corresponding frequency information is usually extracted by the Fourier transform of the original data (Fig. 5b, c). We can clearly see two different frequency signal peaks at 2.5 MHz and 14.7 MHz. It is worth noting that the BAI-based polymer was tested at the same solid weight and parameter settings, so its data are comparable. According to the relationship between the Larmor frequency of protons (ω_N) and the strength of the external magnetic field $\boldsymbol{B_0}$[72]:

$$\boldsymbol{\omega}_N = \frac{\gamma_N}{2\pi}\boldsymbol{B}_0 \tag{6}$$

where γ_N is the gyromagnetic ratio of nuclear spins, $\boldsymbol{B_0}$ used in the experiment is 0.3458 T. The magnetic atoms in BAI-based polymers include H, N, F, and Cl, and their γ_N are 267.519×10^6 Hz·T^{-1}, 19.331×10^6 Hz·T^{-1}, 251.662×10^6 Hz·T^{-1}, and 26.251×10^6 Hz·T^{-1}, respectively. From the above formula and data, we extract the Larmor frequencies of ^{1}H, ^{14}N, ^{19}F, and ^{35}Cl as 14.7 MHz, 1.05 MHz, 13.86 MHz and 1.45 MHz, respectively. Accordingly, the precession frequency at 14.7 MHz in Fig. 5c can be confirmed as being derived from the H atom. As for the Larmor frequencies of N and Cl atoms, they are very close and likely to be the source of the signal peak centred at 2.5 MHz. Since PBAI-V, P2ClBAI-V, and PFClBAI-V all have a strong oscillation frequency at 2.5 MHz, the influence of Cl atoms on spin modulation can be excluded. Moreover, N atoms commonly possess nuclear quadrupole moments[74–76], and thus exhibit multiple quantum transitions of different frequencies (as shown in Fig. 5d), which can lead to frequency broadening in the Fourier spectrum. For the above analysis, it can be concluded that all signals from 0.5 MHz to 5.0 MHz are contributed by N atoms. From Fig. 5c, it is worth noting that the modulation intensity of N atoms is much higher than H atoms, which means N atoms play a more obvious effect on HFI. Particularly, N atoms in BAI-based polymers are located closely to the conjugated center of BAI unit, The relatively high spin intensity around the N atom in BAI-based polymers shows a robust spin-modulated signal, while the spin modulation peak of the H atom mainly comes from the H atom on the side of the BAI skeleton, and the coupling effect provided by the H atom on the TVT unit is very weak. Therefore, we have a reason to infer that the halogen substitution at the margin of conjugated center plays a very tiny and even negligible effect on the spin relaxation.

In order to further demonstrate this conjecture, the spin density and HFI measurements of H_2Pc and PDPP-TT (both of them contain N and H atoms, their chemical structure can be seen in Supplementary Fig. 12) have been provided as shown in Supplementary Fig. 13 and Fig. 5c. The modulation intensity of N and H atoms in these two molecules are slightly different from that of BAI-based polymers. For PDPP-TT (see Supplementary Fig. 13), the spin density is mainly distributed around the N atom, and a certain amount of spin density exists in the thieno[3, 2-b]thiophene (TT) unit, which indicates the H atoms on the TT unit also contribute to HFI. Therefore, compared with the BAI-based polymers, the spin modulation intensity of the H atom in the ESEEM spectrum of PDPP-TT is slightly increased. As for H_2Pc, the spin density of H_2Pc (see Supplementary Fig. 13) is distributed throughout the molecule, and there are 16 H atoms at the edge of the molecule. Therefore, the spin modulation intensity of the H atom is more robust than that of the N atom.

According to the above experimental and theoretical analysis, we need to point that N atoms play a crucial role in spin relaxation in the molecules that contain N atoms. For molecules that only contain C, H, and O elements, the analysis of hyperfine interactions is relatively simple. The H atom has a relatively fast spin modulation frequency. When the spin-polarized carriers injected by ferromagnetic electrodes are transported along the main chain of these molecules, the magnetic coupling from the H atom at the edge of the molecules will result in rapid spin flipping and spin polarization loss[16,29]. However, for OSCs with more complex molecular structural units, such as bay-annulated indigo (BAI), diketopyrrolopyrrole (DPP), isoindigo (IID), naphthalenediimide (NDI) and other amide derivatives OSCs, N atoms have a recurring presence, especially in the conjugated skeleton of the molecules. In this case, the spin relaxation environments in such molecules become more complex, and the investigation on spin relaxation mechanisms will be more challenging. When N atoms occupy the central position of the conjugated skeleton of the molecule, the propagation of spin-polarized carriers in disordered materials is easily subject to robust magnetic interaction from N atoms, inducing the spin relaxation of electrons; the corresponding sketch of spin-polarized carriers transport in BAI-based polymers has been shown in Fig. 5e. In fact, most of the studies on the spin relaxation of organic materials focus on H atoms. In contrast, the role of N atoms is often underestimated or even ignored.

This study investigated the effects of halogen substitution at the edge of the conjugated center on the spin relaxation environment and transport properties of BAI-based polymers. After introducing F and Cl atoms to the edge of the BAI polymer, it is surprisingly found that the carrier mobility of the materials increased by an order of magnitude while its spin lifetime only showed a tiny amount decrease, and eventually the spin diffusion length of BAI-based polymer increased from 64 nm to 247 nm, a record-high value so far. Spin relaxation and their microscopic interactions within molecular structures have been researched, and we found the effects of halogen atoms located at the margin of the molecular conjugated center play an even negligible effect on both SOC and HFI. As a result, an edge substitution strategy can be summarized for guiding molecular structure design towards improving the spin diffusion length of OSCs, whose core characteristic is to substitute atoms far from the centralized region of spin density (commonly the conjugated center) of the molecules. This study proposes a feasible and efficient strategy for the design of OSCs and provides new credible experimental and theoretical guidance for the study of spin relaxation mechanisms and microscopic interactions in organic spintronics.

Methods

Materials and synthesis

The **7a**, **7b**, and **7c** are designed according to the halogenated-edge substitution. The synthetic methods are presented in the Supplementary Information. The H_2Pc and PDPP-TT were purchased from TCI (Shanghai) Development Co., Ltd. and Derthon Optoelectronic Materials Science Technology Co LTD, respectively, and do not require further purification. The ferromagnetic metals (Co and $Ni_{80}Fe_{20}$) were all purchased from Lesker Co., and deposited by e-beam evaporation with the low-temperature deposition technology. The ITO glass was purchased from Wuhan Jinghui Electronic Technology Co., Ltd.

EPR measurements

The EPR spectra were acquired using a Bruker Elexsys E500-T. ESR data acquisition parameters: microwave power 1 mW (23 dB), microwave frequency 9.4 GHz, modulation amplitude 2 gauss, time constant 40.96 ms, and conversion time 40.96 ms. All samples are in a solid film state and are directly loaded into natural quartz tubes for testing at room temperature. Pulse EPR experiments were conducted at X-band frequency on a CIQTEK EPR100 spectrometer. The central magnetic field used for the T_1 and T_2 tests was 345.8 mT. The pulse lengths of π/2 and π are 11 ns and 18.5 ns, respectively. The τ values of both inversion recovery sequence and Hahn echo sequence are 400 ns. For 3P-ESEEM, the mixing time T is stepped up, starting from 170 ns with a step size of 16 ns, to obtain the time-domain spectrum. The delay τ is fixed at 150 ns. The central magnetic field positions of H_2Pc and PDPP-TT are 348 mT and 340 mT, respectively. The EPR spectra of H_2Pc and PDPP-TT can be seen in Supplementary Fig. 14.

Density Functional Theory (DFT) Calculations

All calculations were carried out with the Gaussian 16 software. The CAM-B3LYP functional and 6–31 G* basis set were adopted for all calculations. The DFT-D3 dispersion correction with BJ-damping was applied to improve the calculation accuracy[77–79]. The atomic coordinates of **7a**, **7b**, and **7c** are shown in Supplementary Tables 3, 4, and 5, respectively.

Device fabrication and measurements

The SCLC device was prepared on a glass substrate with 110 nm ITO. The substrate was ultrasonic rinsed with deionized water, ethanol

and trichloride for 2 h and then dried with nitrogen before the device was made. The PBAI-V/P2ClBAI-V/PFClBAI-V was dissolved in chloroform with a concentration of 25 mg/mL and then deposited on the device by spin coating with a thickness of 100 nm in a nitrogen glove box. Subsequently, a 1.1 nm thick LiF was deposited onto the organic layer at a rate of 0.2 Å/s with a shadow mask. Then, 100 nm-thick Al electrodes were deposited as cross-bar layout to the bottom electrodes at the rate of 0.8 Å/s. Finally, the carrier mobilities were extracted using the Keithley 4200 semiconductor analysis system by the SCLC method. The organic spin valves with multilayer vertical structures were prepared on Si/SiO_2 substrate. The substrate was ultrasonic rinsed with deionized water, isopropyl alcohol, and acetone for 1 h and then dried with nitrogen before device fabrication. The Co electrodes were prepared at a rate of ~ 1 Å/s by high vacuum electron beam evaporation with a shadow mask. The Al layer (1.7 nm) was deposited at a rate of 0.3 Å/s and immediately oxidized by air plasma to form a leak-AlO_x layer. Subsequently, PBAI-V/P2ClBAI-V/PFClBAI-V was dissolved in chloroform with a concentration of 8 mg/mL and then deposited on the device by spinning coating with a thickness of 50 nm in a nitrogen glove box. Finally, A low-temperature deposition technique was used to deposit 12 nm NiFe onto the organic layer at a rate of 0.7 Å/s with a shadow mask. The effective area of the prepared organic spin valve is 0.2 mm^2. Supplementary Fig. 15 shows the optical picture of BAI-based polymers spin valve and the thickness of the organic layer was measured by the Spectroscopic Ellipsometer (SE-VE-L from Wuhan Eoptics Technology Co. Ltd). The magnetoresistance is tested through a vacuum magnetic-field probe station (CRX-EM-HF from Lake Shore Cryotronics Co., Ltd.) with a four-probe method. The calculation formula of magnetoresistance (*MR*) signal: $MR = (R_{AP} - R_P)/R_{AP} \times 100\%$, where R_{AP} and R_P are high and low resistances, respectively. The cross-section of the spin valve was prepared by the standard focused ion beam method (Ion-Electron Dual Beam system, FEI Strata DB235), where 100-nm Al was deposited on the device surface to protect the surface during cutting. The cross-section TEM images were obtained using an FEI G2 F30 operating at 300 kV.

Data availability

All data needed to evaluate the conclusions in the paper are present in the paper and/or the Supplementary Information. Source data are provided with this paper.

References

1. Fert, A. Nobel lecture: origin, development, and future of spintronics. *Rev. Mod. Phys.* **80**, 1517–1530 (2008).
2. Grünberg, P. A. Nobel lecture: from spin waves to giant magnetoresistance and beyond. *Rev. Mod. Phys.* **80**, 1531–1540 (2008).
3. Xiong, Z. H., Wu, D., Vardeny, Z. V. & Shi, J. Giant magnetoresistance in organic spin-valves. *Nature* **427**, 821–824 (2004).
4. Szulczewski, G., Sanvito, S. & Coey, M. A spin of their own. *Nat. Mater.* **8**, 693–695 (2009).
5. Sarma, S. D. Spintronics: Fundamentals and applications. *Rev. Mod. Phys.* **76**, 88 (2004).
6. Guo, L., Gu, X., Zhu, X. & Sun, X. Recent advances in molecular spintronics: multifunctional spintronic devices. *Adv. Mater.* **31**, 1805355 (2019).
7. Jang, H. & Richter, C. A. Organic spin-valves and beyond: spin injection and transport in organic semiconductors and the effect of interfacial engineering. *Adv. Mater.* **29**, 1602739 (2017).
8. Barraud, C. et al. Unravelling the role of the interface for spin injection into organic semiconductors. *Nat. Phys.* **6**, 615–620 (2010).
9. Luo, Z. et al. Revealing the key role of molecular packing on interface spin polarization at two-dimensional limit in spintronic devices. *Sci. Adv.* **9**, eade9126 (2023).
10. Sun, D., Ehrenfreund, E. & Valy Vardeny, Z. The first decade of organic spintronics research. *Chem. Commun.* **50**, 1781–1793 (2014).
11. Li, D. & Yu, G. Innovation of materials, devices, and functionalized interfaces in organic spintronics. *Adv. Funct. Mater.* **31**, 2100550 (2021).
12. Schott, S. et al. Polaron spin dynamics in high-mobility polymeric semiconductors. *Nat. Phys.* **15**, 814–822 (2019).
13. Wang, J. et al. Spin-optoelectronic devices based on hybrid organic-inorganic trihalide perovskites. *Nat. Commun.* **10**, 129 (2019).
14. Tsurumi, J. et al. Coexistence of ultra-long spin relaxation time and coherent charge transport in organic single-crystal semiconductors. *Nat. Phys.* **13**, 994–998 (2017).
15. Schott, S. et al. Tuning the effective spin-orbit coupling in molecular semiconductors. *Nat. Commun.* **8**, 15200 (2017).
16. Nguyen, T. D. et al. Isotope effect in spin response of π-conjugated polymer films and devices. *Nat. Mater.* **9**, 345–352 (2010).
17. Bobbert, P. A., Wagemans, W., van Oost, F. W. A., Koopmans, B. & Wohlgenannt, M. Theory for spin diffusion in disordered organic semiconductors. *Phys. Rev. Lett.* **102**, 156604 (2009).
18. Nuccio, L. et al. Importance of spin-orbit interaction for the electron spin relaxation in organic semiconductors. *Phys. Rev. Lett.* **110**, 216602 (2013).
19. Dediu, V. A., Hueso, L. E., Bergenti, I. & Taliani, C. Spin routes in organic semiconductors. *Nat. Mater.* **8**, 707–716 (2009).
20. Raman, K. V. et al. Interface-engineered templates for molecular spin memory devices. *Nature* **493**, 509–513 (2013).
21. Nguyen, T. D., Ehrenfreund, E. & Vardeny, Z. V. Spin-polarized light-emitting diode based on an organic bipolar spin Valve. *Science* **337**, 204–209 (2012).
22. Sun, X. et al. A molecular spin-photovoltaic device. *Science* **357**, 677–680 (2017).
23. Wang, S.-J. et al. Long spin diffusion lengths in doped conjugated polymers due to enhanced exchange coupling. *Nat. Electron.* **2**, 98–107 (2019).
24. Kim, K. et al. Chiral-phonon-activated spin seebeck effect. *Nat. Mater.* **22**, 322–328 (2023).
25. Rocha, A. R. et al. Towards molecular spintronics. *Nat. Mater.* **4**, 335–339 (2005).
26. Hu, B. & Wu, Y. Tuning magnetoresistance between positive and negative values in organic semiconductors. *Nat. Mater.* **6**, 985–991 (2007).
27. Watanabe, S. et al. Polaron spin current transport in organic semiconductors. *Nat. Phys.* **10**, 308–313 (2014).
28. Yang, X. et al. Organic semiconductors for room-temperature spin valves. *ACS Mater. Lett.* **4**, 805–814 (2022).
29. Nguyen, T. D. et al. Isotope effect in the spin response of aluminum tris(8-hydroxyquinoline) based devices. *Phys. Rev. B* **85**, 245437 (2012).
30. Nguyen, T. D. et al. The hyperfine interaction role in the spin response of π-conjugated polymer films and spin valve devices. *Synth. Met.* **161**, 598–603 (2011).
31. Delage-Laurin, L. et al. Overhauser dynamic nuclear polarization with selectively deuterated BDPA radicals. *J. Am. Chem. Soc.* **143**, 20281–20290 (2021).
32. Fratini, S., Nikolka, M., Salleo, A., Schweicher, G. & Sirringhaus, H. Charge transport in high-mobility conjugated polymers and molecular semiconductors. *Nat. Mater.* **19**, 491–502 (2020).
33. Sirringhaus, H. 25th anniversary article: organic field-effect transistors: the path beyond amorphous silicon. *Adv. Mater.* **26**, 1319–1335 (2014).
34. Zhao, Z. et al. High-performance, air-stable field-effect transistors based on heteroatom-substituted naphthalenediimide-benzothiadiazole copolymers exhibiting ultrahigh

electron mobility up to 8.5 cm V^{-1} s^{-1}. *Adv. Mater.* **29**, 1602410 (2017).
35. Song, Y. et al. *N* -doped nonalternant nanoribbons with excellent nonlinear optical performance. *Angew. Chem. Int. Ed.* **62**, e202306418 (2023).
36. Wang, Y., Hasegawa, T., Matsumoto, H., Mori, T. & Michinobu, T. High-performance n-channel organic transistors using high-molecular-weight electron-deficient copolymers and amine-tailed self-assembled monolayers. *Adv. Mater.* **30**, 1707164 (2018).
37. Huang, J. et al. Diazaisoindigo-based polymers with high-performance charge-transport properties: from computational screening to experimental characterization. *Chem. Mater.* **28**, 2209–2218 (2016).
38. McNellis, E. R., Schott, S., Sirringhaus, H. & Sinova, J. Molecular tuning of the magnetic response in organic semiconductors. *Phys. Rev. Mater.* **2**, 074405 (2018).
39. Lei, T. et al. Ambipolar polymer field-effect transistors based on fluorinated isoindigo: high performance and improved ambient stability. *J. Am. Chem. Soc.* **134**, 20025–20028 (2012).
40. Kawashima, K. et al. Implication of fluorine atom on electronic properties, ordering structures, and photovoltaic performance in naphthobisthiadiazole-based semiconducting polymers. *J. Am. Chem. Soc.* **138**, 10265–10275 (2016).
41. Lei, T. et al. Chlorination as a useful method to modulate conjugated polymers: balanced and ambient-stable ambipolar high-performance field-effect transistors and inverters based on chlorinated isoindigo polymers. *Chem. Sci.* **4**, 2447 (2013).
42. Kang, S.-H. et al. Chlorinated 2,1,3-benzothiadiazole-based polymers for organic field-effect transistors. *Macromolecules* **50**, 4649–4657 (2017).
43. He, B. et al. New form of an old natural dye: bay-annulated indigo (BAI) as an excellent electron accepting unit for high performance organic semiconductors. *J. Am. Chem. Soc.* **136**, 15093–15101 (2014).
44. Kolaczkowski, M. A. & Liu, Y. Functional organic semiconductors based on bay-annulated indigo (BAI). *Chem. Rec.* **19**, 1062–1077 (2019).
45. Yang, J. et al. High-performance ambipolar polymers based on electron-withdrawing group substituted bay-annulated indigo. *Adv. Funct. Mater.* **29**, 1804839 (2019).
46. Yang, J. et al. A multihalogenation strategy for ambipolar transistors and high-gain inverters with good noise margin. *Sci. Bull.* **67**, 1849–1853 (2022).
47. Malissa, H. et al. Room-temperature coupling between electrical current and nuclear spins in OLEDs. *Science* **345**, 1487–1490 (2014).
48. Von Kugelgen, S. et al. Spectral addressability in a modular two qubit system. *J. Am. Chem. Soc.* **143**, 8069–8077 (2021).
49. Slota, M. et al. Magnetic edge states and coherent manipulation of graphene nanoribbons. *Nature* **557**, 691–695 (2018).
50. Lombardi, F. et al. Quantum units from the topological engineering of molecular graphenoids. *Science* **366**, 1107–1110 (2019).
51. Jiang, S., Yue, F., Wang, S. & Wu, D. Recent advances in spin transport in organic semiconductors. *Sci. China Phys. Mech. Astron.* **56**, 142–150 (2013).
52. Sun, X. et al. Active morphology control for concomitant long distance spin transport and photoresponse in a single organic device. *Adv. Mater.* **28**, 2609–2615 (2016).
53. Zhang, X. et al. Observation of a large spin-dependent transport length in organic spin valves at room temperature. *Nat. Commun.* **4**, 1392 (2013).
54. Santos, T. S. et al. Room-temperature tunnel magnetoresistance and spin-polarized tunneling through an organic semiconductor barrier. *Phys. Rev. Lett.* **98**, 016601 (2007).
55. Zhang, X. et al. Magnetoresistance effect in rubrene-based spin valves at room temperature. *ACS Appl. Mater. Interfaces* **7**, 4685–4692 (2015).
56. Majumdar, S. et al. Application of regioregular polythiophene in spintronic devices: effect of interface. *Appl. Phys. Lett.* **89**, 122114 (2006).
57. Sun, X. et al. Room-temperature air-stable spin transport in bathocuproine-based spin valves. *Nat. Commun.* **4**, 2794 (2013).
58. Mooser, S., Cooper, J. F. K., Banger, K. K., Wunderlich, J. & Sirringhaus, H. Spin injection and transport in a solution-processed organic semiconductor at room temperature. *Phys. Rev. B* **85**, 235202 (2012).
59. Kawasugi, Y., Ujino, T. & Tada, H. Room-temperature magnetoresistance in organic spin-valves based on a Co2MnSi Heusler alloy. *Org. Electron.* **14**, 3186–3189 (2013).
60. Li, F., Li, T., Chen, F. & Zhang, F. Excellent spin transport in spin valves based on the conjugated polymer with high carrier mobility. *Sci. Rep.* **5**, 9355 (2015).
61. Jiang, S. W. et al. Tuning carrier mobility without spin transport degrading in copper-phthalocyanine. *Appl. Phys. Lett.* **107**, 042407 (2015).
62. Geng, R. et al. Engineering of spin injection and spin transport in organic spin valves using π-conjugated polymer brushes. *Adv. Funct. Mater.* **26**, 3999–4006 (2016).
63. Zhang, X. et al. Room temperature magnetoresistance effects in ferroelectric poly(vinylidene fluoride) spin valves. *J. Mater. Chem. C.* **5**, 5055–5062 (2017).
64. Bairagi, K. et al. Room-temperature operation of a p-type molecular spin photovoltaic device on a transparent substrate. *Adv. Mater.* **32**, 1906908 (2020).
65. Geng, R. et al. Effect of charge localization on the effective hyperfine interaction in organic semiconducting polymers. *Phys. Rev. Lett.* **120**, 086602 (2018).
66. Huang, Y. et al. Unraveling the crucial role of trace oxygen in organic semiconductors. *Nat. Commun.* **15**, 626 (2024).
67. Chen, X.-X. et al. High-mobility semiconducting polymers with different spin ground states. *Nat. Commun.* **13**, 2258 (2022).
68. Han, H. et al. Aromatic stacking mediated spin–spin coupling in cyclophane-assembled diradicals. *J. Am. Chem. Soc.* **143**, 17690–17700 (2021).
69. London, A. E. et al. A high-spin ground-state donor-acceptor conjugated polymer. *Sci. Adv.* **5**, eaav2336 (2019).
70. Willer, M., Granwehr, J., Forrer, J. & Schweiger, A. Two-dimensional nuclear-zeeman-resolved electron spin echo envelope modulation (NZ-ESEEM) spectroscopy. *J. Magn. Reson.* **133**, 46–52 (1998).
71. Xu, J. et al. Magnetic sensitivity of cryptochrome 4 from a migratory songbird. *Nature* **594**, 535–540 (2021).
72. Schweiger, A. & Jeschke, G. *Principles of Pulse Electron Paramagnetic Resonance*. (Oxford University Press, Oxford, 2001).
73. Burstein, D. Stimulated echoes: description, applications, practical hints. *Concepts Magn. Reson.* **8**, 269–278 (1996).
74. Dicus, M. M. et al. Binding of histidine in the $(Cys)_3$ $(His)_1$ -coordinated [2Fe–2S] cluster of human mitoNEET. *J. Am. Chem. Soc.* **132**, 2037–2049 (2010).
75. Doorslaer, S. V., Bachmann, R. & Schweiger, A. A Pulse EPR and ENDOR investigation of the electronic and geometric structure of cobaltous tetraphenylporphyrin(Pyridine). *J. Phys. Chem. A* **103**, 5446–5455 (1999).
76. Xu, S. A supramolecular metalloenzyme possessing robust oxidase-mimetic catalytic function. *Nat. Commun.* **14**, 4040 (2023).
77. Jakobsen, P. & Jensen, F. Probing basis set requirements for calculating hyperfine coupling constants. *J. Chem. Phys.* **151**, 174107 (2019).
78. Grimme, S., Ehrlich, S. & Goerigk, L. Effect of the damping function in dispersion corrected density functional theory. *J. Comput. Chem.* **32**, 1456–1465 (2011).
79. Becke, A. D. Density-functional thermochemistry. III. The role of exact exchange. *J. Chem. Phys.* **98**, 5648–5652 (1993).

Acknowledgements
This work was financially supported by the Strategic Priority Research Program of CAS (XDB0520000, Y.G. and X.S.; XDB0770000, X.S.), the National Natural Science Foundation of China (U22A6002 and 82151305, Y.G.; 52250008, 52050171, 22175047, W2411042, 52303225, X.S.; 52103203, 52473170, L.G.; 52103338 R.Z.), the CAS Project for Young Scientists in Basic Research (YSBR-053), the CAS-Croucher Scheme for Joint Laboratories, the CAS Cooperation Project (121111KYSB20200036, Y.G.), the Beijing Nova Program (20220484173, Y.G.; 20240484551, L.G.), the Beijing Natural Science Foundation (Grant Nos. 4222087, 2222086, X.S.), the State-Funded Postdoctoral Fellows Program of China (Grant No. GZC20230635, 2024T170203, Y.Q.), the CAS Pioneer Hundred Talents Program (X.S.), startup fund provided by the Institute of Chemistry, Chinese Academy of Sciences (J.L.).

Author contributions
X.Y., A.G. and J.Y. co-completed the experimental part. J.C., K. M., and R. D. helped for the EPR experiments and analysis; Y.Q. and S.H. helped for the SCLC experiments; R. D., J.L. and H.Y. provided instrumentation and data analysis for ESEEM testing; W.S., M.Z., and R.Z. helped in data analysis; X.Y., L.G. and Y.G. co-wrote this paper; Y.G., X.S., and Y.L. designed and supervised the work. All the authors contributed to the results, analysis, discussion and manuscript preparation.

Competing interests
The authors declare no competing interests.

Additional information
Supplementary information The online version contains supplementary material available at https://doi.org/10.1038/s41467-024-52770-z.

Correspondence and requests for materials should be addressed to Lidan Guo, Xiangnan Sun, Yunqi Liu or Yunlong Guo.

Peer review information *Nature Communications* thanks Ting Lei and the other, anonymous, reviewer(s) for their contribution to the peer review of this work. A peer review file is available.